CMS Physics Analysis Summary

Contact: cms-pag-conveners-higgs@cern.ch 2017/03/19

Search for pair production of Higgs bosons in the two tau leptons and two bottom quarks final state using proton-proton collisions at $\sqrt{s} = 13$ TeV

The CMS Collaboration

Abstract

A search for the production of Higgs boson pairs in proton-proton collisions at a centre of mass energy of 13 TeV is presented, making use of a data integrated luminosity of 35.9 fb^{-1} collected with the CMS detector at the LHC. Final states with one Higgs boson decaying into two tau leptons and the other one decaying into two bottom quarks are explored to investigate both the resonant and non-resonant production mechanisms. The observed data are well described by standard model processes and no evidence for a signal contribution is found. For resonant production, upper limits at 95% confidence level are set on the production cross section of Higgs boson pairs as a function of the resonance mass, and are interpreted in the context of the minimal supersymmetric standard model. For non-resonant production, upper limits on the production cross section constrain the parameter space for anomalous Higgs boson couplings. The observed (expected) limit corresponds to about 28 (25) times the prediction of the standard model.

1 Introduction

The discovery of the Higgs boson (H) by the ATLAS and CMS Collaborations [1, 2] was a major step towards improving the understanding of the mechanism of electroweak symmetry breaking (EWSB). With the mass of the H boson now precisely determined [3], the structure of the Higgs scalar field potential and the Higgs boson self-couplings are precisely predicted in the standard model (SM). While measured properties are so far consistent with the expectation from the SM predictions [4], the measurement of the Higgs boson self-couplings provides an independent test of the SM and allows to verify that the Brout-Englert-Higgs mechanism is truly responsible for the EWSB by giving access to the determination of the Higgs scalar field potential shape.

The trilinear self-coupling of the Higgs boson (λ_{HHH}) can be extracted from the measurement of the Higgs boson pair production cross section. In the SM, for proton-proton (pp) collisions at the LHC, this process occurs mainly via gluon fusion and involves either couplings of the Higgs boson to virtual fermions in a quantum loop, or the λ_{HHH} coupling itself, with the two processes interfering destructively. The SM prediction for the cross section is $\sigma_{\mathrm{HH}} = 33.49^{+4.3}_{-6.0}(\mathrm{scale}) \pm 2.1(\mathrm{PDF}) \pm 2.3(\alpha_{\mathrm{S}})$ fb [5]. This value was computed at the next-to-next-to-leading order (NNLO) of the theoretical perturbative calculation, including next-to-next-to leading logarithm (NNLL) corrections and finite top quark mass effects.

Beyond the standard model (BSM) physics effects can appear either via anomalous couplings of the Higgs boson or via new particles that can be directly produced or enter in the quantum loop at production. The experimental signature would be an enhancement of the Higgs boson pair production cross section at a specific invariant mass value (resonant production) or over the whole invariant mass spectrum (non resonant production).

The resonant production is predicted by many extensions of the SM such as the Singlet model [6–8], the Two-Higgs Doublet Model (2HDM) [9], the minimal supersymmetric standard model (MSSM) [10, 11], and the Warped Extra Dimensions (WED) [12, 13] model. Although the physics motivations and the phenomenology of these theories are very different, the signal is represented as a CP-even scalar particle (S) decaying into a Higgs boson pair, with an intrinsic width that is often negligible with respect to the detector resolution.

In the non resonant case, the BSM physics is modelled with an effective Lagrangian by extending the SM Lagrangian with dimension-6 operators [14].The Higgs boson coupling to the top quark, y_{t}, and the trilinear coupling λ_{HHH} are modified, and three additional couplings c_2, c_{2g}, and c_g are introduced and represent respectively the interactions of a top pair with a Higgs boson pair, of a gluon pair with a Higgs boson pair, and of a gluon pair with a single Higgs boson. Anomalous y_{t} and λ_{HHH} couplings are investigated in this search, while the other couplings are assumed to be zero.

In this Letter we present a search for Higgs boson pair production in the final state where one Higgs boson decays to a b quark pair and the other decays to a τ lepton pair. This corresponds to a combined branching fraction of 7.3% for a Higgs boson mass of 125 GeV. Three final states of the τ lepton pair are considered: one of the two τ leptons is required to decay into hadrons and a neutrino (τ_{h}), while the other can decay either in the same final state, or into an electron (τ_{e}) or a muon (τ_{μ}) and neutrinos. Together, these three final states include more than 85% of the decays of the $\tau\tau$ system and are the most sensitive ones for this search.

Previous searches for the production of Higgs boson pairs were performed by both the ATLAS [15–18] and CMS [19–25] collaborations using the LHC data collected at $\sqrt{s} = 8$ TeV and $\sqrt{s} = 13$ TeV. This search is based on the previous results at $\sqrt{s} = 13$ TeV in the bb$\tau\tau$ final

state [24, 25] and benefits of the larger integrated luminosity analyzed. Optimized τ lepton candidate identification and isolation, improved event categorization, and a more sensitive discriminating variable have been introduced and result in an improvement of the sensitivity of the search with respect to the previous results.

2 The CMS Detector

The central feature of the CMS apparatus is a superconducting solenoid of 6 m internal diameter, providing a magnetic field of 3.8 T. Within the solenoid volume are a silicon pixel and strip tracker, a lead tungstate crystal electromagnetic calorimeter (ECAL), and a brass and scintillator hadron calorimeter (HCAL), each composed of a barrel and two endcap sections. Forward calorimeters extend the pseudorapidity coverage provided by the barrel and endcap detectors. Muons are identified in gas-ionization detectors embedded in the steel flux-return yoke outside the solenoid. Events of interest are selected using a two-tiered trigger system [26]. The first level (L1), composed of custom hardware processors, uses information from the calorimeters and muon detectors to select events at a rate of around 100 kHz within a time interval of less than 4 μs. The second level, known as the high-level trigger (HLT), consists of a farm of processors running a version of the full event reconstruction software optimized for fast processing, and reduces the event rate to less than 1 kHz before data storage. A more detailed description of the CMS detector, together with a definition of the coordinate system used and the relevant kinematic variables, can be found in Ref. [27].

3 Physics processes modeling

Monte Carlo (MC) samples of resonant and non-resonant Higgs boson pair production via gluon fusion are generated with MADGRAPH_aMC@NLO [28]. In the case of resonant production, separate samples are generated for resonance mass values ranging from 250 to 900 GeV. In the case of non-resonant production, separate MC samples are generated for different values of the effective Lagrangian couplings, including the couplings predicted by the SM [29, 30]. An event weight determined as a function of the generated HH pair kinematics is applied to these samples to model signals corresponding to additional points in the effective Lagrangian parametrization.

Backgrounds arising from $Z/\gamma^* \to \ell\ell$ and $W \to \ell\nu_\ell$ in association with jets (with $\ell = e, \mu, \tau$), di-boson production (WW, ZZ, and WZ), and SM single Higgs production are simulated with MADGRAPH at the leading order precision of the theoretical calculation (LO), while the single-t and $t\bar{t}$ backgrounds are simulated with POWHEG [31, 32]. The NNPDF3.0 [33] parton distributions set is used. In order to increase the number of simulated events that satisfy the requirements detailed in Section 4, the Z/γ^* and W processes are simulated in exclusive regions of multiplicity, flavor, and momentum scalar sums of partons emitted at the matrix element level.

The $t\bar{t}$, $Z/\gamma^* \to \ell\ell$ and $W \to \ell\nu_\ell$ are normalized to their theoretical cross section at the next-to-next-to leading order precision (NNLO), and the single-t, single Higgs, and di-bosons samples are normalized to their cross sections at the next-to leading order (NLO).

4 Object reconstruction and event selection

In order to reconstruct an $HH \to bb\tau\tau$ event, e, μ, and τ leptons, the jets originating from the two b quarks, and the imbalance in the transverse momentum in the event p_T^{miss}, must be

identified.

The particle-flow event algorithm [34, 35] reconstructs and identifies each individual particle with an optimized combination of information from the various elements of the CMS detector. The energy of electrons is determined from a combination of the electron momentum at the primary interaction vertex as determined by the tracker, the energy of the corresponding ECAL cluster, and the energy sum of all bremsstrahlung photons spatially compatible with originating from the electron track. The energy of muons is obtained from the curvature of the corresponding track. The energy of charged hadrons is determined from a combination of their momentum measured in the tracker and the matching ECAL and HCAL energy deposits, corrected for zero-suppression effects and for the response function of the calorimeters to hadronic showers. Finally, the energy of neutral hadrons is obtained from the corresponding corrected ECAL and HCAL energy. Complex objects, such as τ_h, jets, and the missing transverse momentum vector $\boldsymbol{p}_T^{\text{miss}}$ are reconstructed from PF candidates. For each event, hadronic jets are clustered from PF candidates with the infrared and collinear safe anti-k_T algorithm, operated with the distance parameter R of 0.4 and 0.8. These jets are denoted as "ak4" and "ak8" in the following. The jet momentum is determined as the vectorial sum of all particle momenta in this jet, and is found in the simulation to be within 5 to 10% of the true momentum over the whole p_T spectrum and detector acceptance. Jet energy corrections are derived from the simulation, and are confirmed with in situ measurements using the energy balance of dijet and photon plus jet events [36].

Events in the $bb\tau_\mu\tau_h$ ($bb\tau_e\tau_h$) final state have been recorded using a set of triggers that require the presence of a muon (electron) in the event. The events thus selected are required to contain a reconstructed muon (electron) [37, 38] of $p_T > 23(27)$ GeV and $|\eta| < 2.1$ and a reconstructed τ_h candidate [39] of $p_T > 20$ GeV and $|\eta| < 2.3$. The muon (electron) candidate must satisfy the relative isolation requirement $I_l^{rel} < 0.15(0.1)$, while the τ_h candidate must satisfy the "medium" working point of a multivariate isolation discriminant. Additional discriminators are applied to reject electrons and muons erroneously reconstructed as a τ_h candidate [39].

The trigger used for the $bb\tau_h\tau_h$ channel requires the presence of two τ_h candidates in the event. The events selected with this trigger must contain two reconstructed τ_h candidates of $p_T > 45$ GeV and $|\eta| < 2.1$. Both candidates are required to pass the "medium" working point of the multivariate isolation discriminant [39]. Discriminators suppressing prompt electrons and muons are applied to both τ_h candidates.

For all the three final states, the two selected leptons are required to have opposite electric charge. Events containing additional isolated muons or electrons are rejected to reduce the Drell-Yan background contribution.

The events selected with the previous criteria are required to have two additional ak4 jets with $p_T > 20$ GeV and $|\eta| < 2.4$. In the case of Higgs boson pair production via a resonance of mass 700 GeV or higher, the two jets originating from the $H \to bb$ partially overlap due to the high Lorentz boost of the Higgs boson. The two jets are reconstructed at the same time as two separate ak4 jets and as a single ak8 jet for a sizable fraction of the events. The usage of the ak8 algorithm combined with substructure techniques [40] provides a clear separation of the signal topology against the $t\bar{t}$ background, where the two jets are typically more spatially separated and not reconstructed as an ak8 jet.

An event is classified as "boosted" if it contains an ak8 jet of invariant mass larger than 30 GeV that is composed of two sub-jets that are each geometrically matched to one of the selected ak4 jets ($\Delta R\,(\text{ak4}, \text{subjet}) < 0.4$, where $\Delta R = \sqrt{\Delta\eta^2 + \Delta\varphi^2}$ denotes the spatial separation of the

jet candidates). The event is classified as "resolved" if this requirement is not satisfied. Such categorization of the events improves the sensitivity of the search for resonance masses above 700 GeV.

The Combined Secondary Vertex [41] algorithm is applied on the selected jets to identify those originating from a b quark and reduce the contribution from the multijet background where jets are initiated by light quarks or gluon radiation. A "loose" and a "medium" working point of the b-tag discriminator are used in this search. The efficiency and rate of erroneous b jets identification of this working point are about 60% (80%) and 1% (10%) respectively for the "medium" ("loose") working point.

Jets reconstructed in events classified as "resolved" are defined as b-tagged if they satisfy the "medium" working point of the b-tag algorithm. The events are classified into two groups according to the number of b-tagged jets: the group with at least two b-tagged jets (2b) has the best sensitivity, and the one with exactly one b-tagged jet (1b1j) allows to increase the signal acceptance and constrain the systematic uncertainties. Jets reconstructed in the events classified as "boosted" are required to satisfy the "loose" working point of the b-tag discriminator.

After object selection and classification, the kinematic information of the events is exploited to reduce the contribution from background processes. The invariant mass of the two τ lepton candidates, $m_{\tau\tau}$, is reconstructed using a dynamical likelihood technique [42] that combines the kinematics of the two visible candidates and the missing transverse momentum in the event. The bb invariant mass, m_{bb}, is estimated from the two selected jets candidates for "resolved" topologies and from the invariant mass of the ak8 jet with the soft drop jet grooming algorithm [43] for "boosted" topologies. In the "resolved" case, the events are required to satisfy the condition:

$$\frac{(m_{\tau\tau} - 116\,\text{GeV})^2}{(35\,\text{GeV})^2} + \frac{(m_{bb} - 111\,\text{GeV})^2}{(45\,\text{GeV})^2} < 1 \tag{1}$$

where the values of 35 and 45 GeV have been chosen according to the resolution on the invariant mass for the $\tau\tau$ and bb objects and 116 and 111 GeV correspond to the position of the expected reconstructed 125 GeV Higgs boson peak in the $m_{\tau\tau}$ and m_{bb} distributions respectively. In the "boosted" case the events are required to satisfy:

$$\begin{aligned} 80\,\text{GeV} < m_{\tau\tau} < 160\,\text{GeV} \\ 90\,\text{GeV} < m_{bb} < 160\,\text{GeV} \end{aligned} \tag{2}$$

In addition to the previous requirements, a multivariate discriminant is applied on $\tau_\mu\tau_h$ and $\tau_e\tau_h$ selected events to identify and reject the $t\bar{t}$ process, that is the most important source of background in these two final states. The discriminant consists in a Boosted Decision Tree (BDT) [44, 45] that is trained on a set of simulated signal and background events to identify the kinematic differences of the two processes and assigns to every selected event a number that defines its compatibility with a signal or background topology. Two separate BDT trainings are performed to achieve an optimal performance for all the signal processes studied. One training is performed using resonant signals with mass $m_S \leq 350\,\text{GeV}$ as input. Eight variables are used as input to the discriminant training because of their good separation power between signal and background: $\Delta\varphi(H_{bb}, H_{\tau\tau})$, $\Delta\varphi(H_{\tau\tau}, p_T^{miss})$, $\Delta\varphi(H_{bb}, p_T^{miss})$, $\Delta R(b,b) \cdot p_T(H_{bb})$, $\Delta R(\ell, \tau_h) \cdot p_T(H_{\tau\tau})$, $m_T(\ell)$, $m_T(\tau_h)$, and $\Delta\varphi(\ell, p_T^{miss})$. Here ℓ refers to either the selected electron or muon, H_{bb} and $H_{\tau\tau}$ denote the H boson candidates reconstructed

from the two leptons and the two jets respectively, and $\mathrm{m_T}(\ell) = \sqrt{(p_\mathrm{T}^\ell + E_\mathrm{T}^\mathrm{miss})^2 - (\boldsymbol{p}_\mathrm{T}^\ell \cdot \boldsymbol{p}_\mathbf{T}^\mathrm{miss})^2}$ denotes the transverse mass of the selected lepton candidate (the definition is equivalent for $\mathrm{m_T}(\tau_\mathrm{h})$). The same training is used both for the search of resonant HH production up to $\mathrm{m_S} = 350\,\mathrm{GeV}$ and for the search of non-resonant HH production. It has been verified that this training performs optimally on non-resonant signals and that there is no performance loss in comparison to a dedicated training on non-resonant signals. Different selections on the BDT discriminator output are applied in the two searches to maximize the sensitivity: these selections correspond to a rejection of the $\mathrm{t\bar{t}}$ background of approximately 90% and 70% for the resonant and non-resonant searches respectively. A second training is performed on resonant signals of mass $\mathrm{m_S} > 350\,\mathrm{GeV}$. The variables used as input to this training are the same as in the previous case, but replacing $\Delta R(\mathrm{b},\mathrm{b}) \cdot p_\mathrm{T}(\mathrm{H_{bb}})$ and $\Delta R(\ell, \tau_\mathrm{h}) \cdot p_\mathrm{T}(\mathrm{H}_{\tau\tau})$ with $\Delta R(\mathrm{b},\mathrm{b})$ and $\Delta R(\ell, \tau_\mathrm{h})$. The selection on the BDT output is chosen to maximize the sensitivity and corresponds to a rejection of the $\mathrm{t\bar{t}}$ background of approximately 90%.

In the resonant search, the invariant mass of the two visible τ lepton decay products and the two selected b jets m_HH, is used to search for a possible signal over the expected background event distribution. In order to improve the resolution and consequently enhance the sensitivity of the analysis, the invariant mass is reconstructed using a kinematic fit ($m_\mathrm{HH}^\mathrm{KinFit}$) that is detailed in Ref. [46]. The fit is based on the four momenta of the τ and b candidates and on the missing transverse momentum vector in the event, and is performed under the hypothesis of two 125 GeV Higgs bosons decaying into a b quark pair and a τ lepton pair.

The stransverse mass or $\mathrm{M_{T2}}$ is used for the search of a non-resonant signal. It is defined as

$$\mathrm{M_{T2}}\left(m_B, m_{B'}, \boldsymbol{b}_\mathrm{T}, \boldsymbol{b}'_\mathrm{T}, \boldsymbol{p}_\mathrm{T}{}^\Sigma, m_C, m_{C'}\right) = \min_{\boldsymbol{c}_\mathrm{T}+\boldsymbol{c}'_\mathrm{T}=\boldsymbol{p}_\mathrm{T}{}^\Sigma} \left\{\max\left(m_\mathrm{T}, m'_\mathrm{T}\right)\right\} \tag{3}$$

where the transverse mass m_T is defined as

$$m_\mathrm{T}\left(\boldsymbol{b}_\mathrm{T}, \boldsymbol{c}_\mathrm{T}, m_b, m_c\right) = \sqrt{m_b^2 + m_c^2 + 2\left(e_b e_c - \boldsymbol{b}_\mathrm{T} \cdot \boldsymbol{c}_\mathrm{T}\right)} \tag{4}$$

and the "transverse energy" e is defined as

$$e = \sqrt{m^2 + \boldsymbol{p}_\mathrm{T}{}^2} \tag{5}$$

This variable was introduced for SUSY searches involving invisible particles in the final state [47, 48] and later proposed for HH searches in the $\mathrm{bb}\tau\tau$ final state [49], and we use the computation methods implemented in [50]. In our application to the HH search, the quantities in the Equation (3) are defined as indicated in [49]: B, B' denote the two b-jets and C, C' denote the two tau leptons, $\boldsymbol{p}_\mathrm{T}{}^\Sigma = \boldsymbol{p}_\mathrm{T}{}^{vis}(\tau_1) + \boldsymbol{p}_\mathrm{T}{}^{vis}(\tau_2) + \boldsymbol{p}_\mathbf{T}^\mathrm{miss}$, $m_C = m^{vis}(\tau_1)$ and $m_{C'} = m^{vis}(\tau_2)$.

The $\mathrm{M_{T2}}$ variable has by construction a large discriminating power of the HH signal against the $\mathrm{t\bar{t}}$ background. For the irreducible background process $\mathrm{t\bar{t}} \to \mathrm{bb\,WW} \to \mathrm{bb}\,\tau\nu_\tau\tau\nu_\tau$, $\mathrm{M_{T2}}$ is bounded superiorly at the top quark mass m_t, while it can assume larger values for the HH signal. Detector resolution effects and other decay modes of the $\mathrm{t\bar{t}}$ system (e.g. jets from the W boson misidentified as two τ_h) result in an extension of the tail of the $\mathrm{M_{T2}}$ $\mathrm{t\bar{t}}$ background distribution beyond the m_t value.

5 Background estimation

The main background sources that contaminate the signal region are due to $Z/\gamma^* \to \ell\ell$ production, $t\bar{t}$ production and multi-jet QCD events.

The $Z/\gamma^* \to \ell\ell$ background contribution is estimated using the MC simulation, where the LO modeling of jet emission in the Z/γ^* process is known to be imperfect. Therefore, corrections factors are calculated using data in three regions defined by the presence of two isolated, opposite sign muons compatible with the hypothesis of a $Z \to \mu\mu$ decay and by the presence of 0, 1, or ≥ 2 b-tagged jets respectively. Three correction factors are derived for the Z/γ^* production in association with 0, 1, or ≥ 2 b-quarks emitted at matrix element level and applied in the signal regions.

The multijet background is determined from data in a jet-enriched region defined by requiring that the two selected lepton candidates have the same electric charge. The yield is obtained from this same-sign (SS) region, where all the other selections are applied as in the signal region. The events in this region are scaled by the ratio of opposite-sign (OS) to SS event yields obtained in a multijet enriched region with inverted τ lepton isolation. The contributions of other backgrounds are subtracted in the OS and SS regions based on MC predictions. The shape of the multijet background is estimated using the events in a SS region with relaxed τ lepton isolation, after subtracting the other background contributions based on their MC predictions.

The $t\bar{t}$, single top, single Higgs, W boson in association with jets, and di-boson processes are estimated using the simulation.

6 Systematic uncertainties

The effects due to an imperfect knowledge of the detector response, discrepancies between simulation and data, and limited knowledge of the background and signal processes are accounted for in the analysis as systematic uncertainties. They are separately treated as "normalization" uncertainties or "shape" ones; the first type affects the number of expected events in the signal region, while the second type affects their distributions.

6.1 Normalization uncertainties

- The integrated luminosity is known with an uncertainty of 2.6%, assumed to be fully correlated among the various final states under study. This value is obtained from dedicated Van-der-Meer scans and stability of detector response during the data taking. The uncertainty is applied to the signal and to $t\bar{t}$, W+jets, single top, single Higgs, and di-boson backgrounds, while it is not applied on the multijet and Z+jets backgrounds because they are estimated or corrected from data. For the same reason, the following uncertainties, related to the final state objects reconstruction, are considered only for background processes modeled with the simulation.
- Electron, muon, and τ lepton trigger, reconstruction and identification efficiencies are measured using $Z \to ee$, $Z \to \mu\mu$, and $Z \to \tau\tau \to \mu\nu_\mu\tau_h\nu_\tau$ events collected at $\sqrt{s} = 13\,\text{TeV}$. The corresponding uncertainties are considered as uncorrelated among the final states and account for about 3% for electrons, 2% for muons and 6% for τ leptons.
- An uncertainty on each τ_h candidate coming from τ energy scale knowledge weighs about 3% for each τ_h candidate, and impacts on the overall normalization ranging

Table 1: Systematic uncertainties affecting the normalization of the different processes.

Systematic	value	processes
Luminosity	2.6%	all but multijet, $Z/\gamma^* \to \ell\ell$
Lepton trigger and reconstruction	2-6%	all but multijet
τ energy scale	3-10%	all
Jet energy scale	2-4%	all
b-tag efficiency	2-6%	all
MC cross-section	1-10%	all but multijet, $Z/\gamma^* \to \ell\ell$
$Z/\gamma^* \to \ell\ell$ SF uncertainty	0.1-2.5%	$Z/\gamma^* \to \ell\ell$
multijet normalization	5-30%	multijet
scale unc.	$+4/-6\%$	signals
PDF variation	3%	signals

from 3% to 10% depending on the considered process. This effect is fully correlated with a corresponding shape uncertainty on the distribution of M_{T2} and M_{HH}^{KinFit}.

- Uncertainties arising from the imperfect knowledge of the jet and b-jet measured energy have an impact of about 2% for the signal processes and 4% for the backgrounds.
- Uncertainties on b-tagging efficiency in the simulation are evaluated as function of jet p_T and η and result in an average value of 2-6% for the samples with true b-jets in the final state.
- For the tt, W+jets, single top, single Higgs, and di-boson backgrounds, uncertainties due to the imperfect knowledge of the process normalizations and simulation are considered and range from 1% to 10%.
- The uncertainties on the three correction factors for the $Z/\gamma^* \to \ell\ell$ background are propagated from the control region to the signal region, taking into account the correlation between the three factors.
- The uncertainty on the multijet background normalization is estimated by propagating the statistical uncertainties on the number of events used for its determination in the region with the sign requirement inverted, as described in Section 3, and ranges between 5% and 30% depending on the final state and category.
- The uncertainties in the signal modeling arising from scales and PDF variations result in an uncertainty on the signal processes normalization of +4%/-6% and 3% respectively.

The values of the systematic uncertainties are summarized in Table 1.

6.2 Shape uncertainties

- The uncertainty in the distribution of $t\bar{t}$ event is taken into account due to the imperfect knowledge of the differential p_T distribution of simulated events.
- Uncertainties due to the limited number of simulated events or due to the statistical fluctuations of events in the multijet control region are taken into account. These uncertainties are uncorrelated across bins in the individual templated shapes.
- Uncertainties due to the τ and jet energy scales are taken into account and are fully correlated with the associated normalization uncertainties. Uncertainties on other objects scales have a negligible impact on the simulated event distributions and are not taken into account.

7 Results

Figures 1, 2, and 3 show the distributions of events in the $\tau_\mu\tau_h$, $\tau_e\tau_h$, and $\tau_h\tau_h$ respectively for the different event categories in the signal regions defined for this search. A binned maximum likelihood fit is performed simultaneously on these distributions. In the absence of evidence for a signal, we set 95% confidence level (CL) upper limits on the cross section of Higgs boson pair production.

For the non-resonant production mode, limits are set for different hypotheses of anomalous self-coupling and t-quark coupling of the Higgs boson. The deviations from the SM couplings are parametrized using the coefficients $k_\lambda = \lambda_{HHH}/\lambda_{HHH}^{SM}$ and $k_t = y_t/y_t^{SM}$. The signal kinematics depending on the ratio of the two couplings, 95% CL upper limits are set as a function of k_λ/k_t, assuming the other BSM couplings to be zero. The result is shown in Figure 4a and the exclusion is compared with the theoretical prediction of the cross section for $k_t = 1$ and $k_t = 2$. Including the theoretical uncertainties on the cross section, the observed upper limit corresponds to approximately 28 times the SM prediction, while the expected one is about 25 times the SM prediction. These upper limits are used to set constraints on anomalous k_λ and k_t couplings as shown in Figure 4b, where the other BSM couplings are assumed to be equal to zero.

For the resonant production mode, limits are set as a function of the mass of the resonance m_S under the hypothesis that its intrinsic width is negligible compared to the experimental resolution. The observed and expected 95% CL limits are shown in Figure 5a. These model-independent limits are interpreted in the hMSSM scenario [51, 52], that is a parametrization of the MSSM that considers the observed 125 GeV Higgs boson as the lighter scalar predicted from the model (usually denoted as h in the context of the model), while the resonance of mass m_S represents the heavier CP-even scalar (usually denoted as H in the context of the model). Excluded regions as a function of the m_A and $\tan\beta$ parameters of the model are shown in Figure 5b.

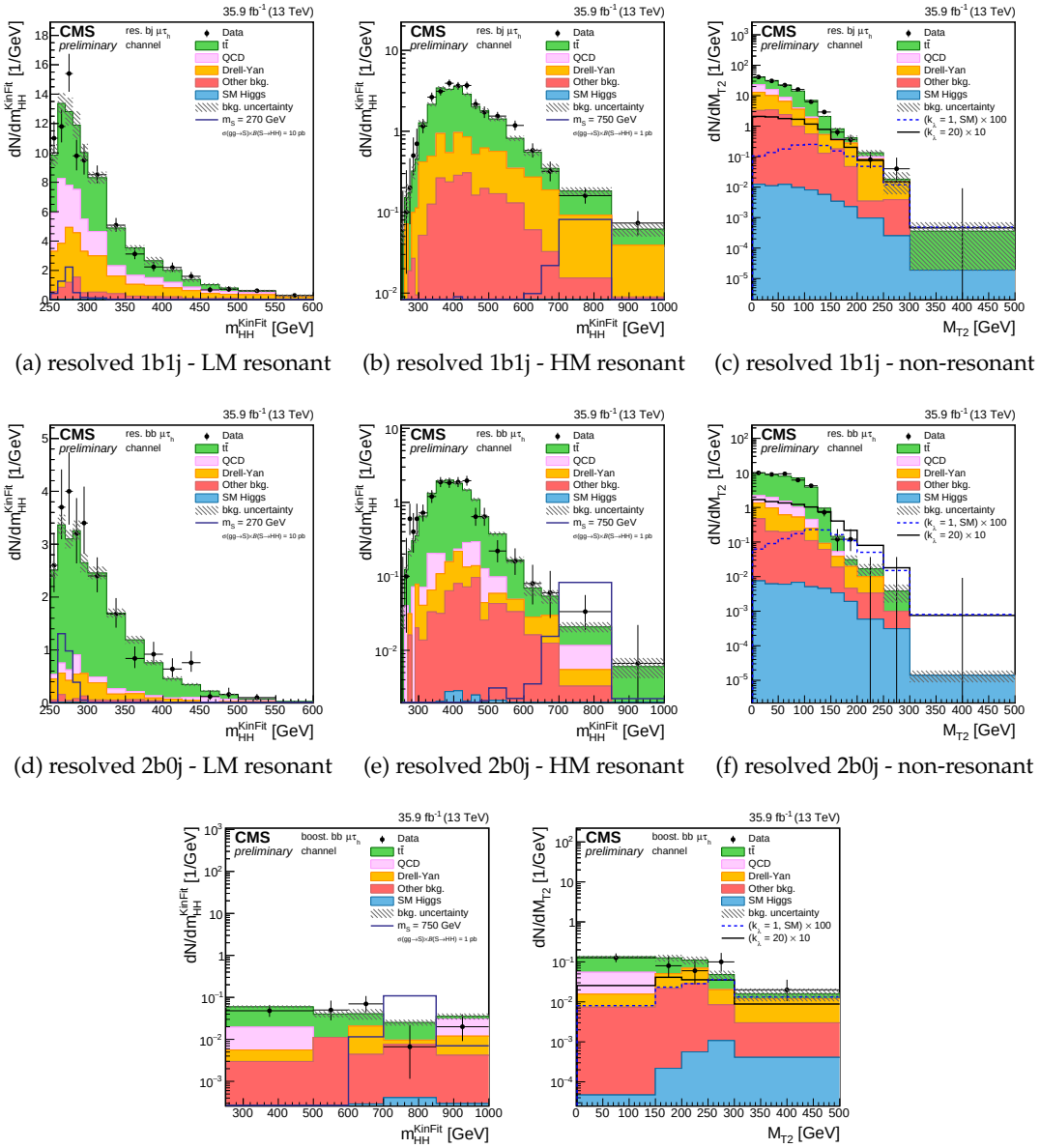

(a) resolved 1b1j - LM resonant (b) resolved 1b1j - HM resonant (c) resolved 1b1j - non-resonant

(d) resolved 2b0j - LM resonant (e) resolved 2b0j - HM resonant (f) resolved 2b0j - non-resonant

(g) boosted - resonant (h) boosted - non-resonant

Figure 1: Distributions of the events observed in the signal regions of the $\tau_\mu\tau_h$ final state. The first, second, and third row show the resolved 1b1j, 2b0j, and boosted regions respectively. Figures (a),(b),(d),(e),(g) show the distribution of the M_{HH}^{KinFit}variable and Figures (c),(f),(h) show the distribution of the M_{T2} variable. Points with error bars represent the data and shaded histograms represent the backgrounds, while the solid lines represent the expected signal yields and are not stacked to the background histograms. The dashed areas correspond to the systematic uncertainty band of the background estimates. Distributions and nuisances are shown after the fit to the observed data.

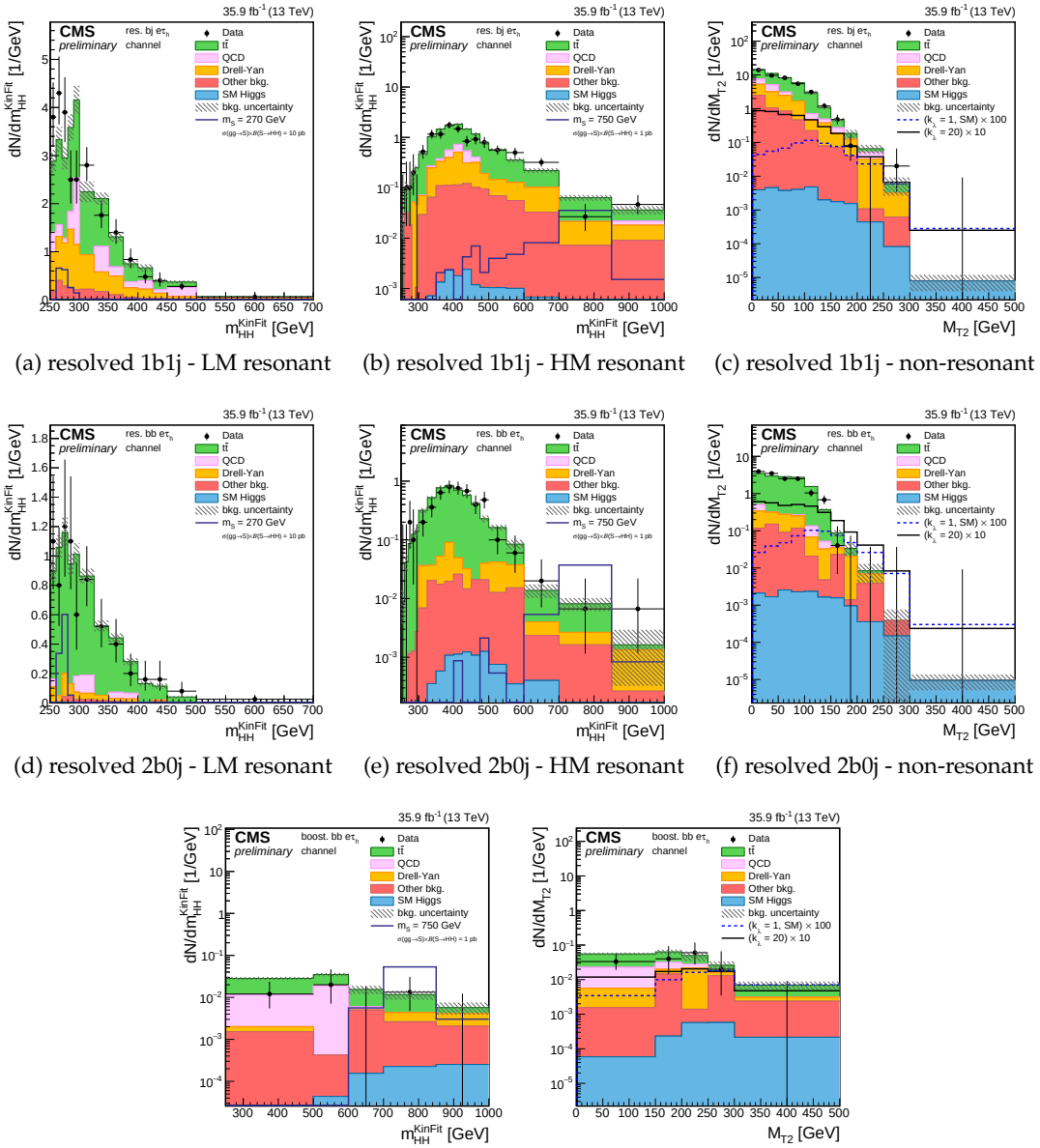

(a) resolved 1b1j - LM resonant (b) resolved 1b1j - HM resonant (c) resolved 1b1j - non-resonant

(d) resolved 2b0j - LM resonant (e) resolved 2b0j - HM resonant (f) resolved 2b0j - non-resonant

(g) boosted - resonant (h) boosted - non-resonant

Figure 2: Distributions of the events observed in the signal regions of the $\tau_e\tau_h$ final state. The first, second, and third row show the resolved 1b1j, 2b0j, and boosted regions respectively. Figures (a),(b),(d),(e),(g) show the distribution of the M_{HH}^{KinFit}variable and Figures (c),(f),(h) show the distribution of the M_{T2} variable. Points with error bars represent the data and shaded histograms represent the backgrounds, while the solid lines represent the expected signal yields and are not stacked to the background histograms. The dashed areas correspond to the systematic uncertainty band of the background estimates. Distributions and nuisances are shown after the fit to the observed data.

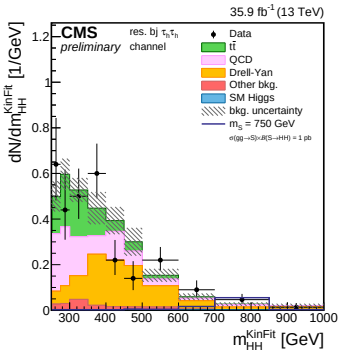

(a) resolved 1b1j - resonant

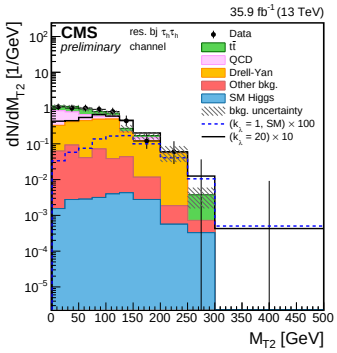

(b) resolved 1b1j - non-resonant

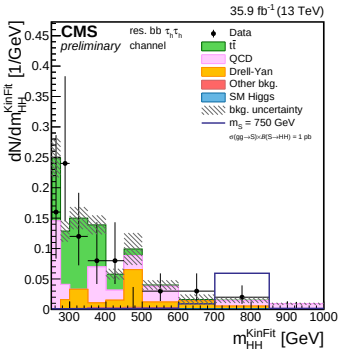

(c) resolved 2b0j - resonant

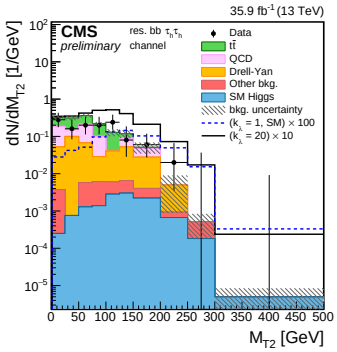

(d) resolved 2b0j - non-resonant

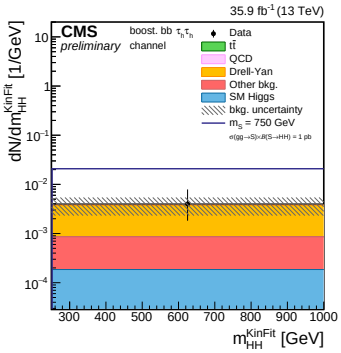

(e) boosted - resonant

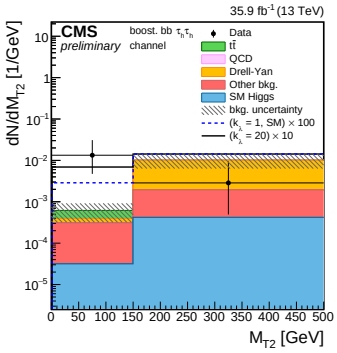

(f) boosted - non-resonant

Figure 3: Distributions of the events observed in the signal regions of the $\tau_h\tau_h$ final state. The first, second, and third row show the resolved 1b1j, 2b0j, and boosted regions respectively. Figures (a),(b),(d),(e) show the distribution of the M_{HH}^{KinFit} variable and Figures (c),(f) show the distribution of the M_{T2} variable. Points with error bars represent the data and shaded histograms represent the backgrounds, while the solid lines represent the expected signal yields and are not stacked to the background histograms. The dashed areas correspond to the systematic uncertainty band of the background estimates. Distributions and nuisances are shown after the fit to the observed data.

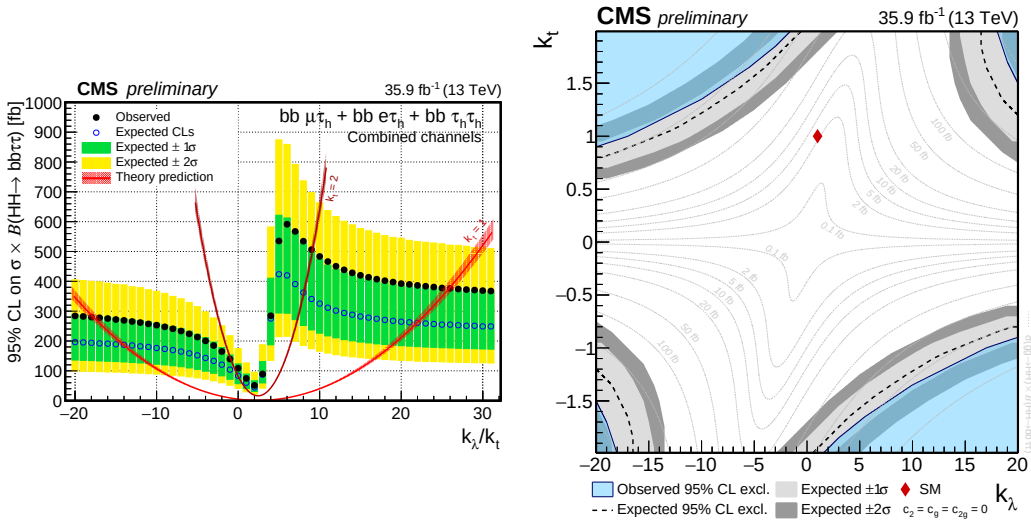

(a) k_λ / k_t scan (b) Exclusion in (k_λ, k_t) plane

Figure 4: (a): observed and expected 95% CL upper limits on cross section times branching fraction as a function of k_λ / k_t. The two red bands show the theoretical cross section expectations and the corresponding uncertainties for $k_t = 1$ and $k_t = 2$. (b): test of k_λ and k_t anomalous couplings. The blue region denotes the parameters excluded at 95% CL with the observed data, while the dashed black line and the gray regions denote the expected exclusions and the 1σ and 2σ bands. The dotted gray lines indicate trajectories in the plane with equal values of cross section times branching fraction that are displayed in the associated labels. The red marker denotes the couplings predicted by the SM. In both figures, the couplings that are not explicitly tested are assumed to correspond to the SM prediction.

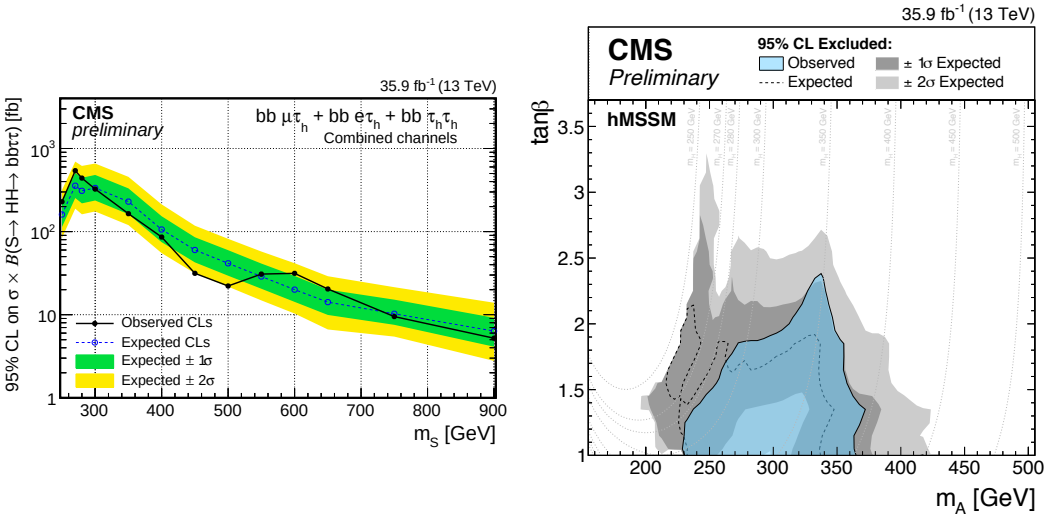

(a) Model independent limit

(b) Interpretation in the hMSSM model

Figure 5: (a) : observed and expected 95% CL upper limits on cross section times branching fraction as a function of the mass of the resonance m_S under the hypothesis that its intrinsic width is negligible with respect to the experimental resolution. (b) : interpretation of the exclusion limit in the context of the hMSSM model, parametrized as a function of the tan β and m_A parameters. In this model, the CP-even lighter scalar is assumed to be the observed 125 GeV Higgs boson and is denoted as h, while the CP-even heavier scalar is denoted as H. The gray dotted lines indicate trajectories in the plane corresponding to the same values of m_H.

8 Conclusions

The search for resonant and non-resonant Higgs boson (HH) production in the $bb\tau\tau$ final state is presented. The search is performed using $35.9\,fb^{-1}$ of data collected in proton-proton collisions at $\sqrt{s} = 13\,TeV$ and uses the three most sensitive decay channels of the τ lepton pair, namely $\tau_\mu\tau_h$, $\tau_e\tau_h$, and $\tau_h\tau_h$. The results are found to be compatible within the uncertainties to the expected SM background contribution, and upper confidence limits on the HH production cross sections are set.

For the non-resonant production mechanism, the theoretical framework of the effective Lagrangian is used to parametrize the cross section as a function of anomalous couplings of the Higgs boson. Upper confidence limits on the HH cross section are derived as a function of $k_\lambda = \lambda_{HHH}/\lambda^{SM}_{HHH}$ and $k_t = y_t/y_t^{SM}$. The 95% CL observed upper limit corresponds to approximately 28 times the theoretical prediction for the SM cross section, and the expected one is about 25 times the SM prediction.

For the resonant production mechanism, upper exclusion limits at 95% CL are derived for the production of a narrow resonance of mass m_S ranging from 250 to 900 GeV. These model independent limits are interpreted in the context of MSSM scenarios where the HH production cross section is parametrized as a function of the m_A and $\tan\beta$ parameters of the model.

References

[1] ATLAS Collaboration, "Observation of a new particle in the search for the Standard Model Higgs boson with the ATLAS detector at the LHC", *Physics Letters B* **716** (2012), no. 1, 1 – 29, doi:10.1016/j.physletb.2012.08.020.

[2] CMS Collaboration, "Observation of a new boson at a mass of 125 GeV with the CMS experiment at the LHC", *Physics Letters B* **716** (2012), no. 1, 30 – 61, doi:10.1016/j.physletb.2012.08.021.

[3] ATLAS, CMS Collaboration, "Combined Measurement of the Higgs Boson Mass in pp Collisions at $\sqrt{s} = 7$ and 8 TeV with the ATLAS and CMS Experiments", *Phys. Rev. Lett.* **114** (2015) 191803, doi:10.1103/PhysRevLett.114.191803, arXiv:1503.07589.

[4] ATLAS, CMS Collaboration, "Measurements of the Higgs boson production and decay rates and constraints on its couplings from a combined ATLAS and CMS analysis of the LHC pp collision data at $\sqrt{s} = 7$ and 8 TeV", *JHEP* **08** (2016) 045, doi:10.1007/JHEP08(2016)045, arXiv:1606.02266.

[5] LHC Higgs Cross Section Working Group Collaboration, "Handbook of LHC Higgs Cross Sections: 4. Deciphering the Nature of the Higgs Sector", arXiv:1610.07922.

[6] T. Binoth and J. J. van der Bij, "Influence of strongly coupled, hidden scalars on Higgs signals", *Z. Phys.* **C75** (1997) 17–25, doi:10.1007/s002880050442, arXiv:hep-ph/9608245.

[7] R. Schabinger and J. D. Wells, "Minimal spontaneously broken hidden sector and its impact on Higgs boson physics at the CERN Large Hadron Collider", *Phys. Rev. D* **72** (Nov, 2005) 093007, doi:10.1103/PhysRevD.72.093007.

[8] B. Patt and F. Wilczek, "Higgs-field Portal into Hidden Sectors", arXiv:hep-ph/0605188.

[9] G. C. Branco et al., "Theory and phenomenology of two-Higgs-doublet models", *Phys. Rept.* **516** (2012) 1–102, doi:10.1016/j.physrep.2012.02.002, arXiv:1106.0034.

[10] P. Fayet, "Supergauge invariant extension of the Higgs mechanism and a model for the electron and its neutrino", *Nuclear Physics B* **90** (1975) 104 – 124, doi:http://dx.doi.org/10.1016/0550-3213(75)90636-7.

[11] P. Fayet, "Spontaneously broken supersymmetric theories of weak, electromagnetic and strong interactions", *Physics Letters B* **69** (1977), no. 4, 489 – 494, doi:http://dx.doi.org/10.1016/0370-2693(77)90852-8.

[12] K. Agashe, H. Davoudiasl, G. Perez, and A. Soni, "Warped gravitons at the CERN LHC and beyond", *Phys. Rev. D* **76** (Aug, 2007) 036006, doi:10.1103/PhysRevD.76.036006.

[13] A. L. Fitzpatrick, J. Kaplan, L. Randall, and L.-T. Wang, "Searching for the Kaluza-Klein graviton in bulk RS models", *JHEP* **09** (2007) 013, doi:10.1088/1126-6708/2007/09/013, arXiv:hep-ph/0701150.

[14] F. Goertz, A. Papaefstathiou, L. L. Yang, and J. Zurita, "Higgs boson pair production in the D=6 extension of the SM", *JHEP* **04** (2015) 167, doi:10.1007/JHEP04(2015)167, arXiv:1410.3471.

[15] ATLAS Collaboration, "Searches for Higgs boson pair production in the $hh \to bb\tau\tau$, $\gamma\gamma WW^*$, $\gamma\gamma bb$, $bbbb$ channels with the ATLAS detector", *Phys. Rev. D* **92** (Nov, 2015) 092004, doi:10.1103/PhysRevD.92.092004.

[16] ATLAS Collaboration, "Search for pair production of Higgs bosons in the $b\bar{b}b\bar{b}$ final state using proton−proton collisions at $\sqrt{s} = 13$ TeV with the ATLAS detector", Technical Report ATLAS-CONF-2016-049, CERN, Geneva, Aug, 2016.

[17] ATLAS Collaboration, "Search for Higgs boson pair production in the final state of $\gamma\gamma WW^*(\to l\nu jj)$ using 13.3 fb^{-1} of pp collision data recorded at $\sqrt{s} = 13$ TeV with the ATLAS detector", Technical Report ATLAS-CONF-2016-071, CERN, Geneva, Aug, 2016.

[18] ATLAS Collaboration, "Search for Higgs boson pair production in the $b\bar{b}\gamma\gamma$ final state using pp collision data at $\sqrt{s} = 13$ TeV with the ATLAS detector", Technical Report ATLAS-CONF-2016-004, CERN, Geneva, Mar, 2016.

[19] CMS Collaboration, "Search for two Higgs bosons in final states containing two photons and two bottom quarks in proton-proton collisions at 8 TeV", *Phys. Rev. D* **94** (Sep, 2016) 052012, doi:10.1103/PhysRevD.94.052012.

[20] CMS Collaboration, "Search for resonant pair production of Higgs bosons decaying to two bottom quark-antiquark pairs in proton-proton collisions at 8 TeV", *Phys. Lett.* **B749** (2015) 560–582, doi:10.1016/j.physletb.2015.08.047, arXiv:1503.04114.

[21] CMS Collaboration, "Search for non-resonant pair production of Higgs bosons in the $b\bar{b}b\bar{b}$ final state with 13 TeV CMS data", Technical Report CMS-PAS-HIG-16-026, CERN, Geneva, 2016.

[22] CMS Collaboration, "Search for H(bb)H(gammagamma) decays at 13TeV", Technical Report CMS-PAS-HIG-16-032, CERN, Geneva, 2016.

[23] CMS Collaboration, "Search for Higgs boson pair production in the $b\bar{b}l\nu l\nu$ final state at $\sqrt{s} = 13$ TeV", Technical Report CMS-PAS-HIG-16-024, CERN, Geneva, 2016.

[24] CMS Collaboration, "Search for non-resonant Higgs boson pair production in the $b\bar{b}\tau^+\tau^-$ final state", CMS Physics Analysis Summary CMS-PAS-HIG-16-028, CERN, 2016.

[25] CMS Collaboration, "Search for resonant Higgs boson pair production in the $b\bar{b}\tau^+\tau^-$ final state", CMS Physics Analysis Summary CMS-PAS-HIG-16-029, CERN, 2016.

[26] CMS Collaboration, "The CMS trigger system", *JINST* **12** (2017) P01020, doi:10.1088/1748-0221/12/01/P01020, arXiv:1609.02366.

[27] CMS Collaboration, "The CMS experiment at the CERN LHC", *JINST* **3** (2008) S08004, doi:10.1088/1748-0221/3/08/S08004.

[28] J. Alwall et al., "The automated computation of tree-level and next-to-leading order differential cross sections, and their matching to parton shower simulations", *Journal of High Energy Physics* **2014** (2014), no. 7, 79, doi:10.1007/JHEP07(2014)079.

[29] A. Carvalho et al., "Higgs Pair Production: Choosing Benchmarks With Cluster Analysis", *JHEP* **04** (2016) 126, doi:10.1007/JHEP04(2016)126, arXiv:1507.02245.

[30] A. Carvalho et al., "Analytical parametrization and shape classification of anomalous HH production in the EFT approach", arXiv:1608.06578.

[31] E. Re, "Single-top Wt-channel production matched with parton showers using the POWHEG method", *Eur. Phys. J.* **C71** (2011) 1547, doi:10.1140/epjc/s10052-011-1547-z, arXiv:1009.2450.

[32] J. M. Campbell, R. K. Ellis, P. Nason, and E. Re, "Top-pair production and decay at NLO matched with parton showers", *Journal of High Energy Physics* **2015** (2015), no. 4, 114, doi:10.1007/JHEP04(2015)114.

[33] NNPDF Collaboration, "Parton distributions for the LHC Run II", *JHEP* **04** (2015) 040, doi:10.1007/JHEP04(2015)040, arXiv:1410.8849.

[34] CMS Collaboration, "Particle-Flow Event Reconstruction in CMS and Performance for Jets, Taus, and MET", CMS Physics Analysis Summary CMS-PAS-PFT-09-001, CERN, 2009.

[35] CMS Collaboration, "Commissioning of the particle-flow event reconstruction with the first LHC collisions recorded in the CMS detector", CMS Physics Analysis Summary CMS-PAS-PFT-10-001, CERN, 2010.

[36] CMS Collaboration, "Determination of jet energy calibration and transverse momentum resolution in CMS", *JINST* **6** (2011) P11002, doi:10.1088/1748-0221/6/11/P11002, arXiv:1107.4277.

[37] CMS Collaboration, "Performance of electron reconstruction and selection with the CMS detector in proton-proton collisions at $\sqrt{s} = 8$ TeV", *JINST* **10** (2015), no. 06, P06005, doi:10.1088/1748-0221/10/06/P06005, arXiv:1502.02701.

[38] CMS Collaboration, "Performance of CMS muon reconstruction in pp collision events at $\sqrt{s} = 7$ TeV", *JINST* **7** (2012) P10002, doi:10.1088/1748-0221/7/10/P10002, arXiv:1206.4071.

[39] CMS Collaboration, "Reconstruction and identification of τ lepton decays to hadrons and ν_τ at CMS", *JINST* **11** (2016), no. 01, P01019, doi:10.1088/1748-0221/11/01/P01019, arXiv:1510.07488.

[40] J. M. Butterworth, A. R. Davison, M. Rubin, and G. P. Salam, "Jet substructure as a new Higgs search channel at the LHC", *Phys. Rev. Lett.* **100** (2008) 242001, doi:10.1103/PhysRevLett.100.242001, arXiv:0802.2470.

[41] CMS Collaboration, "Identification of b-quark jets with the CMS experiment", *JINST* **8** (2013) P04013, doi:10.1088/1748-0221/8/04/P04013, arXiv:1211.4462.

[42] L. Bianchini, J. Conway, E. K. Friis, and C. Veelken, "Reconstruction of the Higgs mass in $H \to \tau\tau$ Events by Dynamical Likelihood techniques", *J. Phys. Conf. Ser.* **513** (2014) 022035, doi:10.1088/1742-6596/513/2/022035.

[43] A. J. Larkoski, S. Marzani, G. Soyez, and J. Thaler, "Soft drop", *Journal of High Energy Physics* **2014** (2014), no. 5, 146, doi:10.1007/JHEP05(2014)146.

[44] A. Hocker et al., "TMVA - Toolkit for Multivariate Data Analysis", *PoS* **ACAT** (2007) 040, arXiv:physics/0703039.

[45] J. H. Friedman, "Greedy function approximation: A gradient boosting machine.", *Ann. Statist.* **29** (10, 2001) 1189–1232, doi:10.1214/aos/1013203451.

[46] CMS Collaboration, "Searches for a heavy scalar boson H decaying to a pair of 125 GeV Higgs bosons hh or for a heavy pseudoscalar boson A decaying to Zh, in the final states with $h \to \tau\tau$", *Phys. Lett.* **B755** (2016) 217–244, doi:10.1016/j.physletb.2016.01.056, arXiv:1510.01181.

[47] C. G. Lester and D. J. Summers, "Measuring masses of semiinvisibly decaying particles pair produced at hadron colliders", *Phys. Lett.* **B463** (1999) 99–103, doi:10.1016/S0370-2693(99)00945-4, arXiv:hep-ph/9906349.

[48] A. Barr, C. Lester, and P. Stephens, "m(T2): The Truth behind the glamour", *J. Phys.* **G29** (2003) 2343–2363, doi:10.1088/0954-3899/29/10/304, arXiv:hep-ph/0304226.

[49] A. J. Barr, M. J. Dolan, C. Englert, and M. Spannowsky, "Di-Higgs final states augMT2ed – selecting *hh* events at the high luminosity LHC", *Phys. Lett.* **B728** (2014) 308–313, doi:10.1016/j.physletb.2013.12.011, arXiv:1309.6318.

[50] C. G. Lester and B. Nachman, "Bisection-based asymmetric MT2 computation: a higher precision calculator than existing symmetric methods", *Journal of High Energy Physics* **2015** (2015), no. 3, 100, doi:10.1007/JHEP03(2015)100.

[51] A. Djouadi et al., "The post-Higgs MSSM scenario: Habemus MSSM?", *Eur. Phys. J.* **C73** (2013) 2650, doi:10.1140/epjc/s10052-013-2650-0, arXiv:1307.5205.

[52] A. Djouadi et al., "Fully covering the MSSM Higgs sector at the LHC", *JHEP* **06** (2015) 168, doi:10.1007/JHEP06(2015)168, arXiv:1502.05653.